J. Appl. Cryst. (1996). **29**, 246–260

Quantitative Analysis of Time-Resolved Laue Diffraction Patterns

ZHONG REN,[a,b] KINGMAN NG,[a*] GLORIA E. O. BORGSTAHL,[c†] ELIZABETH D. GETZOFF[c] AND KEITH MOFFAT[a,b]

[a]*Department of Biochemistry and Molecular Biology, The University of Chicago, 920 East 58th Street, Chicago, IL 60637, USA,* [b]*Consortium for Advanced Radiation Sources, The University of Chicago, 5640 South Ellis Avenue, Chicago, IL 60637, USA, and* [c]*Department of Molecular Biology, The Scripps Research Institute, 10666 North Torrey Pines Road, La Jolla, CA 92037, USA.*
E-mail: renz@vishnu.uchicago.edu

(*Received 5 October 1995; accepted 15 January 1996*)

Abstract

Integration and quantification of time-resolved Laue images poses problems beyond those encountered with static Laue images. The flexible analytical profile-fitting technique [Ren & Moffat (1995). *J. Appl. Cryst.* **28**, 461–481] has been extended to handle the integration of multiple-spot images with two or more exposures at different time points superimposed on a single detector frame but displaced by a small shift. Each Laue pattern on a multiple-spot image can be integrated separately; possible spatial overlaps between adjacent spots from either the same or different exposures can be resolved; streakiness and streakiness anisotropy are allowed to be different for each time point. Various strategies for time-resolved Laue diffraction data collection and processing are compared. Time-resolved Laue images obtained during the relaxation of photoactive yellow protein (PYP) from its photostationary state have been processed by the Laue data reduction package *LaueView*. Continuous laser illumination of PYP crystals establishes a photostationary state and termination of laser illumination starts a relaxation process. However, PYP crystals at the photostationary state are more anisotropically mosaic than those at the ground state, and the mosaicity and its anisotropy vary during the relaxation. Accurate integration of elongated and spatially overlapping spots therefore becomes more difficult. Two data processing strategies have been applied to calculate time-dependent difference Fourier maps of PYP. The first route takes advantage of both the wavelength normalization and the harmonic deconvolution [Ren & Moffat (1995). *J. Appl. Cryst.* **28**, 461–481, 482–493] algorithms. The second is the method of relative percentage changes of structure-factor amplitudes.

1. Introduction

One of the most important applications of Laue diffraction is to the time-resolved study of rapid biochemical reactions in crystals (Cruickshank, Helliwell & Johnson, 1992; Pai, 1992; Hajdu & Andersson, 1993; Ren & Moffat, 1994). This application is based on two major advantages of Laue diffraction: the briefest exposure times and the use of a stationary crystal. Fast time-resolved crystallographic studies may involve very brief exposures, spanning the time range from 1 s down to 50 ps. From a dipole source on a second-generation synchrotron such as the National Synchrotron Light Source (NSLS), even a small protein crystal may require Laue exposure times of only 20 to 100 ms in order to get strong diffraction data (Moffat, Chen, Ng, McRee & Getzoff, 1992). The greatly increased brilliance of third-generation synchrotron sources such as the European Synchrotron Radiation Facility (ESRF) and the Advanced Photon Source (APS) will reduce the exposure time even further and provide an excellent opportunity for investigating rapid biochemical reactions directly by X-ray diffraction techniques at fine time resolution and high spatial resolution.

The Laue diffraction technique suffers from several difficulties (Hajdu & Andersson, 1993; Ren & Moffat, 1995*a*). Laue diffraction patterns are extremely sensitive to crystal mosaicity, which produces elongated, streaky diffraction spots in detector space. Reaction initiation in crystals by techniques such as laser illumination often increases crystal mosaicity and the streakiness of the diffraction patterns (Moffat *et al.*, 1992). Furthermore, crystal mosaicity changes induced by laser illumination or subsequent structural reactions can be both anisotropic and time-dependent (Moffat *et al.*, 1992; Bartunik, Bartunik & Viehmann, 1992). Laue patterns from protein and other macromolecular crystals may have numerous spatial overlaps between adjacent diffraction spots. These complexities make accurate integration of time-resolved Laue patterns more difficult. We have developed a new approach to handle various shapes of Laue diffraction spots using a flexible analytical profile (Ren & Moffat,

* Present address: Lilly Research Laboratories, Eli Lilly and Company, Lilly Corporate Center, Indianapolis, IN 46285, USA.
† Present address: Life Sciences Division, Los Alamos National Laboratory, Los Alamos, NM 87545, USA.

1995*a*). Centimeter-long Laue spots in which the ratio of the longer to the shorter spot dimension is up to 50 : 1 have been successfully integrated (V. Srajer, unpublished results). This analytical approach also allows possible spatial overlaps between adjacent spots to be resolved.

The initial goal of a time-resolved experiment is to obtain accurate and complete difference structure amplitudes $\Delta F_{\mathbf{H}}(t)$, in which the structure amplitude $|\mathbf{F}_{\mathbf{H}}(t)|$ for a reflection $\mathbf{H}=(hkl)$ at a time t after initiation of a structural reaction is compared with the structure amplitude $|\mathbf{F}_{\mathbf{H}}(0)|$ immediately prior to initiation. That is,

$$\Delta F_{\mathbf{H}}(t) = |\mathbf{F}_{\mathbf{H}}(t)| - |\mathbf{F}_{\mathbf{H}}(0)| \quad (1)$$

$$\sigma[\Delta F_{\mathbf{H}}(t)] = \{\sigma^2[|\mathbf{F}_{\mathbf{H}}(t)|] + \sigma^2[|\mathbf{F}_{\mathbf{H}}(0)|]\}^{1/2}, \quad (2)$$

where $\sigma(x)$ is the uncertainty of value x. A complete time-resolved data set is four-dimensional: it spans a unique volume in reciprocal space and time. The design of a time-resolved experiment must consider how best to scan this four-dimensional space, bearing in mind that the values of $\Delta F_{\mathbf{H}}(t)$ are likely to be small and subject to both systematic and random errors. Examples of systematic errors are reaction initiation artifacts such as mosaicity, leading to Laue spot streaking and thermal effects, and scaling errors; and random errors are enhanced by the short exposures and limited number of diffracted photons for each reflection.

The normal method of Laue data processing is to derive and apply the wavelength-dependent correction factors to each integrated intensity and thus to obtain the structure amplitudes *via* a wavelength-normalization strategy (Ren & Moffat, 1995*a*). However, if difference structure-factor amplitudes are the goal rather than structure-factor amplitudes, then the complicated process of wavelength normalization can be circumvented by obtaining the values of $\Delta F_{\mathbf{H}}(t)/|\mathbf{F}_{\mathbf{H}}(0)|$ directly from the Laue intensities (Bilderback, Moffat & Szebenyi, 1984) and combining this with subsidiary measurement of $|\mathbf{F}_{\mathbf{H}}(0)|$ to yield $\Delta F_{\mathbf{H}}$ (Hajdu, Machin, Campbell, Greenhough, Clifton, Zurek, Gover, Johnson & Elder, 1987). In the time-resolved experiment,

$$\begin{aligned}\Delta F_{\mathbf{H}}(t) &= |\mathbf{F}_{\mathbf{H}}(t)| - |\mathbf{F}_{\mathbf{H}}(0)| \\ &= [(|\mathbf{F}_{\mathbf{H}}(t)| - |\mathbf{F}_{\mathbf{H}}(0)|)/|\mathbf{F}_{\mathbf{H}}(0)|]|\mathbf{F}_{\mathbf{H}\,\text{reference}}| \quad (3)\end{aligned}$$

where $|\mathbf{F}_{\mathbf{H}\,\text{reference}}|$ denotes the structure amplitude in the absence of any structural change and may be derived either from a reference monochromatic or Laue data set, or from the time-resolved Laue experiment itself, $|\mathbf{F}_{\mathbf{H}}(0)|$. The term in square brackets is derivable directly from the time-resolved Laue measurements if certain assumptions hold (Bilderback *et al.*, 1984). We denote this second route of Laue data processing as the relative-change route, in contrast to the normal wavelength-normalization route.

In a time-resolved Laue diffraction experiment, the detector can be moved continuously or discontinuously in its plane during the X-ray exposure. This movement may be either physical, in the case of an image plate, or electronic, in the case of a charge-coupled device. For continuous motion, each diffraction spot is elongated into a streak in which position along the streak correlates with time (Moffat, Bilderback, Schildkamp & Volz, 1986; Moffat, 1989). Shrive & Greenhough (1994) have provided a method for integrating such time-resolved images. We consider here a second experimental design in which the detector is always stationary during the exposure but moves discontinuously between exposures. A series of time points is resolved separately at a fixed crystal orientation. Members of this series may be recorded in the conventional way on separate detector frames; we denote these single-spot images, since each frame contains a single diffraction pattern corresponding to one time point, $t \geq 0$. Alternatively, several members of this series may be recorded on a single frame; we denote these multiple-spot or m-spot images with $m \geq 2$, in which each separate diffraction pattern corresponds to a different time point. The m patterns are displaced from each other by motion of the detector between (not during) exposures, again either physically or electronically. Fig. 1 illustrates single-spot, two-spot and four-spot patterns. An entire four-dimensional data set is then acquired by repetition of the experiment at different crystal orientations to span the unique volume in reciprocal space, and at different time points or groups of time points to span the desired time range.

In this paper, we extend our strategy for processing static single-spot Laue images (Ren & Moffat, 1994, 1995*a*,*b*) to multiple-spot time-resolved Laue images. We compare data quality (accuracy and completeness) obtained in both single-spot and multiple-spot approaches, and the wavelength-normalization and relative-change approaches to obtaining difference structure amplitudes. We illustrate these four different data-acquisition and reduction strategies by applying them to time-resolved Laue studies of decay from the photostationary state of photoactive yellow protein, PYP (Ng, Getzoff & Moffat, 1995; Borgstahl, Williams & Getzoff, 1995; Ng, Borgstahl, Ren, Genick, Burke, Pradervand, Schildkamp, McRae, Getzoff & Moffat, 1996). These results are more generally applicable to the optimum design and conduct of time-resolved Laue experiments.

2. Materials and methods

2.1. *Crystals*

Photoactive yellow protein (PYP; Meyer, 1985), isolated from the halophilic bacterium *Ectothiorhodospira halophila*, is a water-soluble 14 kDa photoreceptor protein with a fully reversible photocycle resembling that of sensory rhodopsin II. PYP crystals are in space group $P6_3$ with cell constants $a=b=66.9$ and $c=40.7$ Å

(McRee, Meyer, Cusanovich, Parge & Getzoff, 1986; McRee, Tainer, Meyer, Van Beeumen, Cusanovich & Getzoff, 1989; Borgstahl *et al.*, 1995). PYP crystals have a bright yellow color and can be bleached reversibly as indicated by optical absorption changes. A saturated photostationary state of the crystal can be established *via* continuous laser illumination, and interruption of the illumination starts a relaxation process back down to the ground dark state. We have shown spectroscopically that relaxation from the photostationary state in crystals is biphasic at 269 K with faster and slower components of 5.2 and 1.4 s^{-1} (Ng *et al.*, 1995).

2.2. *Monochromatic data collection*

A monochromatic data set was collected on a Siemens area detector mounted on a Rigaku rotating-anode X-ray generator (Borgstahl *et al.*, 1995). The data set was collected at room temperature and a 0.1° frame width was used. The data set was completed from one PYP crystal with size of 250 × 250 × 500 μm. Data were reduced by the *XENGEN* data-processing package. These monochromatic data to 1.4 Å resolution provide a reference data set of the best quality.

2.3. *Time-resolved Laue data collection*

The process of PYP relaxation from the photostationary state has been measured optically (Ng *et al.*, 1995) and crystallographically on the same crystal at the same time. Laue images were collected corresponding to the ground state (dark) and the excited state. The second, excited-state, exposure spans the period from 2 to 12 ms after interruption of laser illumination that quantitatively populated the saturated photostationary state, here called the excited state. Laue data sets were collected on beamline X26C at the National Synchrotron Light Source (NSLS), Brookhaven National Laboratory (Getzoff, Jones, McRee, Moffat, Ng, Rivers, Schildkamp, Singer, Spanne, Sweet, Teng & Westbrook, 1993). The white X-ray beam is focused by a platinum-coated cylindrical focusing mirror. The storage ring was operated at a current between 230 and 110 mA. A BioCARS Laue bench camera was used to take these Laue photographs. A 150 μm aluminium foil was inserted into the X-ray beam in order to attenuate the X-ray beam at longer wavelengths and to limit X-ray heating of the crystals. The X-ray beam was collimated at 300 μm diameter. The crystal-to-detector distance was set to 200 mm. Fuji HR-III_N imaging plates of size 20.1 × 25.2 cm were used to record the diffraction patterns and a Fuji BAS2000 scanner digitized the diffraction images using the Fuji software supplied. A 100 μm raster size was used. The crystals were mounted in thin-walled glass capillaries. An FTS cooling system bathed the crystal during data collection in a gas stream maintained at 261 K. We found that exposures longer than 30 ms showed X-ray heating artifacts from thermally induced crystal mosaicity and, in accordance with this observation, we calculate that the adiabatic heating rate due to X-ray absorption of this focused white beam is 200 K s^{-1} or 2 K in 10 ms (Chen, 1994). This heating rate is derived from the known incident spectral intensity profile [for example, the spectral intensity at 1.2 Å from this focused X26C beamline is 2×10^{12} photons s^{-1} mm^{-2} (0.1% bandpass)$^{-1}$], the mass-absorption coefficient of the crystal, its volume and its specific heat (assumed to be that of water). We therefore divided the total exposure of 100 to 160 ms into 10 to 16 10 ms subexposures with 30 s intervals in between each subexposure. These multiple subexposures allow sufficient time for thermal equilibration in crystals to take place between individual X-ray subexposures and minimize the peak temperature rise caused by the X-ray shots. Since 10 ms is only a small fraction of the half-time of PYP relaxation kinetics (130 and 500 ms for the faster and the slower components detected optically; Ng *et al.*, 1995), we anticipated that little structure averaging would occur over the duration of the exposure. Reproducibility between subexposures was monitored through the optical absorption spectrum.

2.4. *Integration*

In multiple-spot images, multiple exposures are recorded on one image with a small detector shift (1.5 mm) between each exposure (Moffat *et al.*, 1992). This experimental strategy aims at minimizing the systematic error introduced by frame-to-frame scaling, but it concomitantly decreases the signal-to-noise ratio by a factor given by the number of exposures and increases the number of spatial overlaps. In addition, multiple exposures are often taken under multiple conditions. For example, one spot may be a control, $t = 0$, and the other spots are recorded at different time points t after the reaction initiation. Spots of the same reflection derived from different exposures and time points may have very different shapes and hence require different profiles (Moffat *et al.*, 1992). The analytical profile for single-spot Laue images (Ren & Moffat, 1995*a*) therefore needs to be extended.

We begin by reviewing their approach. In the analytical profile, there are two groups of adjustable parameters. Group 1 parameters are independent of position in detector space. Group 1 has $2 + n$ parameters: p_0, p_b, p_i $(i = 1, 2, \ldots, n)$, where n is the number of adjacent spots spatially overlapping with the desired Laue spot; p_0 describes the scale of the desired spot; p_b is the background level; and p_i $(i = 1, 2, \ldots, n)$ describe the scales of the adjacent spots. Group 1 parameters are determined by profile fitting of every individual spot on the image. Group 2 parameters depend on position in detector space. Group 2 has 13 parameters: a and b are

the dimensions of a spot, which describe the spot streakiness and size; ε is the nonradial streakiness correction; s_a, t_a and s_b, t_b are nonelliptical corrections, able to describe many odd shapes of Laue spots; g_a and g_b are non-Gaussian kurtosis corrections; d_x and d_y are the geometry refinement error corrections; and p_x and p_y are the background slopes around the Laue spot. Group 2 parameters are initially defined by profile fitting of some strong reflections that are not spatially overlapped and then the parameters are modified to form a smooth surface for each across the detector frame. Therefore, final group 2 parameters are fixed within a single detector bin (a small portion of the detector frame) and vary slowly across the entire detector space. Now, since exposures at different time points require different profiles, multiple sets of group 2 parameters are necessary, one for each time point. Thus, multiple parameter surfaces, one for each time point, can be obtained that show the smoothness of the group 2 parameter sets and the differences between them. Spatial-overlap deconvolution is carried out in a manner identical to that for single-spot images, except that now the overlapping profiles can differ. The software system *LaueView*, which incorporates this approach (Ren & Moffat, 1995*a*,*b*), was designed from the outset to handle multiple-spot ($m \leq 10$) images.

2.5. *Difference coefficients for Fourier maps*

A complete time-resolved data set has many subsets, one for each time point. Since each subset can be treated as a static data set, data reduction of a time-resolved data

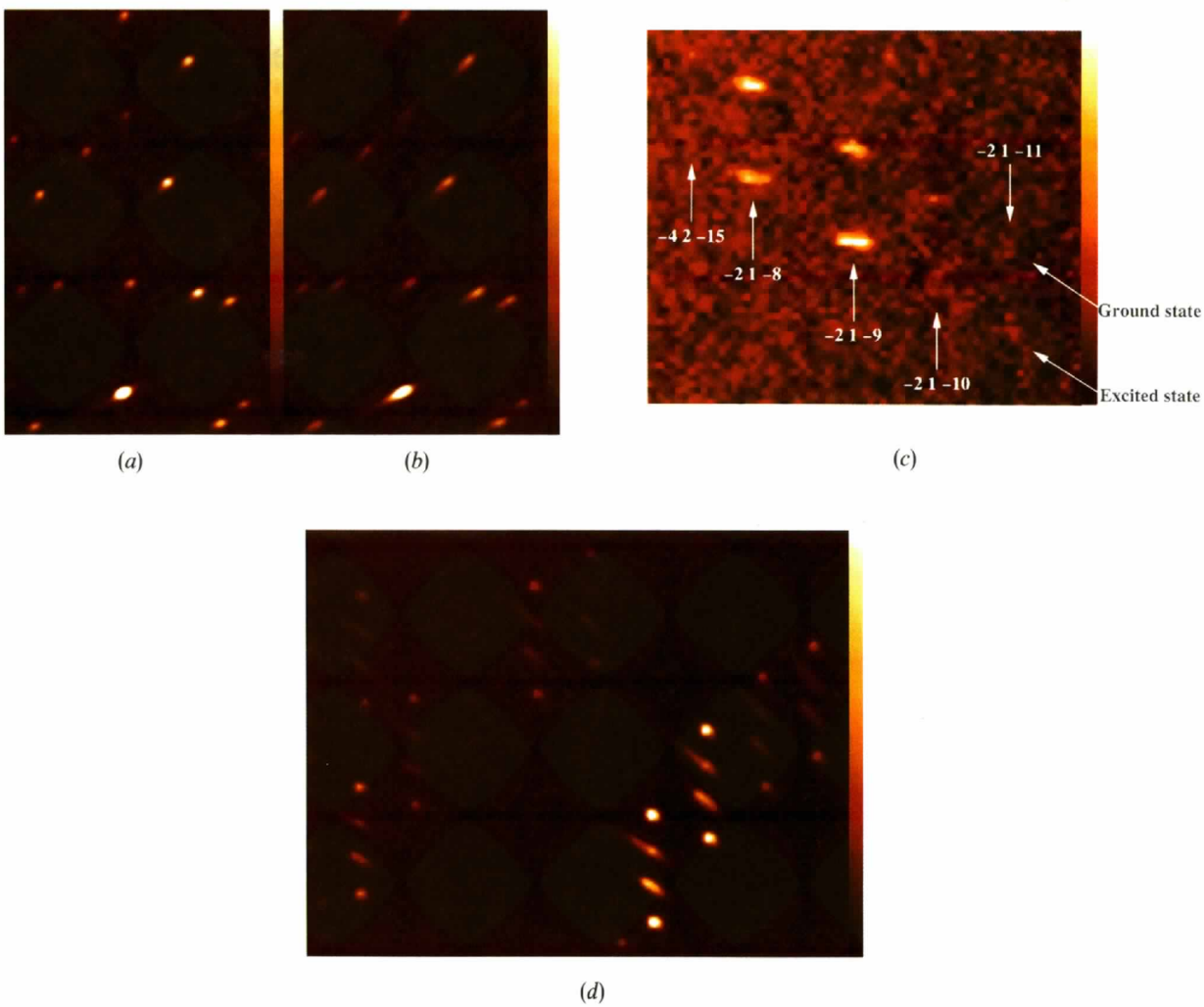

Fig. 1. Examples of one-spot image (*a*) before and (*b*) after laser illumination. (*c*) A portion of a PYP two-spot image. Running diagonally, there are two rows of spots from the ground and excited states as marked. These two diffraction patterns are displaced vertically by 1.5 mm. The indices of each column are also marked on the image. The intensity reversals of the reflections $\bar{2}1\bar{8}$ and $\bar{2}1\bar{9}$ are clearly shown. Some reflections are too weak to be identified by eye. (*d*) Example of a four-spot image. From the top, before any laser illumination, during laser illumination, immediately (2 ms) after laser turned off and 1 s after laser turned off.

set can be carried out as though it were data reduction of multiple static data sets. In particular, harmonic deconvolution (Ren & Moffat, 1995*b*) is directly applicable. Difference Fourier coefficients can be calculated directly *via* this wavelength normalization route [(1) and (2)]. A potential systematic error in this approach could arise from uncertainty of the wavelength normalization curve (λ curve) for each time point. More seriously, systematic errors will be introduced if the λ curves differ for each time point. To avoid this, all subsets at different time points should share one λ curve. That is, we derive one λ curve for multiple subsets just as if they formed a single large data set. The determination of a single λ curve from the large combined data set containing multiple subsets is a slower computational process because of the larger number of data.

The second strategy is to adopt the relative-change route and avoid the wavelength-normalization step. This kind of data-collection strategy requires that every reflection **H** diffracts at all time points and is stimulated throughout by X-rays of the same wavelength. The relative percentage change $\Delta F_{\mathbf{H}i}(t)/|\mathbf{F}_{\mathbf{H}i}(0)|$ of the ith measurement of the single (nonharmonic overlapping) reflection **H** is obtained directly (Bilderback *et al.*, 1984) from the integrated intensities $I_{\mathbf{H}i}$:

$$\begin{aligned}\Delta F_{\mathbf{H}i}(t)/|\mathbf{F}_{\mathbf{H}i}(0)| &= [|\mathbf{F}_{\mathbf{H}i}(t)| - |\mathbf{F}_{\mathbf{H}i}(0)|]/|\mathbf{F}_{\mathbf{H}i}(0)| \\ &= \{[I_{\mathbf{H}i}(t)]^{1/2} \\ &\quad - [I_{\mathbf{H}i}(0)]^{1/2}\}/[I_{\mathbf{H}i}(0)]^{1/2}, \qquad (4)\end{aligned}$$

$$\begin{aligned}\sigma^2[\Delta F_{\mathbf{H}i}(t)/|\mathbf{F}_{\mathbf{H}i}(0)|] &= [|\mathbf{F}_{\mathbf{H}i}(t)|/4|\mathbf{F}_{\mathbf{H}i}(0)|] \\ &\quad \times (\{\sigma^2[I_{\mathbf{H}i}(0)]/I^2_{\mathbf{H}i}(0)\} \\ &\quad + \{\sigma^2[I_{\mathbf{H}i}(t)]/I^2_{\mathbf{H}i}(t)\}), \qquad (5)\end{aligned}$$

where $I_{\mathbf{H}i}(t)$ and $I_{\mathbf{H}i}(0)$ are the integrated intensities of the ith measurement of single reflection **H** for the time point t and the initial time point, respectively. The average $\Delta F_{\mathbf{H}}(t)/|\mathbf{F}_{\mathbf{H}}(0)|$ and its standard deviation $\sigma[\Delta F_{\mathbf{H}}(t)/|\mathbf{F}_{\mathbf{H}}(0)|]$ can be calculated. Difference Fourier coefficients can be obtained if a reference data set is available:

$$\Delta F_{\mathbf{H}}(t) = [\Delta F_{\mathbf{H}}(t)/|\mathbf{F}_{\mathbf{H}}(0)|]|\mathbf{F}_{\mathbf{H}\,\text{reference}}|, \qquad (6)$$

$$\begin{aligned}\sigma[\Delta F_{\mathbf{H}}(t)] &= \Delta F_{\mathbf{H}}(t) \\ &\quad \times (\{\sigma^2[\Delta F_{\mathbf{H}}(t)/|\mathbf{F}_{\mathbf{H}}(0)|]/[\Delta F_{\mathbf{H}}(t)/|\mathbf{F}_{\mathbf{H}}(0)|]^2\} \\ &\quad + [\sigma^2(|\mathbf{F}_{\mathbf{H}\,\text{reference}}|)/|\mathbf{F}_{\mathbf{H}\,\text{reference}}|^2])^{1/2}. \qquad (7)\end{aligned}$$

This relative-change route has several limitations (Moffat, 1989; Moffat & Helliwell, 1989). First, reflections involved in energy overlaps cannot be retrieved in the absence of wavelength normalization, and therefore lower completeness of the data set is inevitable, especially at lower resolution. Second, a reference time point must be collected together with the desired time point under identical experimental conditions including crystal orientation. This increases the total exposure time by a factor of $1/(m-1)$ for m-spot images. Third, if the crystal orientation changes slightly between the desired time points, a systematic error is introduced owing to the concomitant shift of the stimulating X-ray wavelength. Fourth, a large uncertainty in the relative change is associated with a low integrated intensity [(4)], which eventually leads to a large uncertainty in the difference Fourier coefficient [(7)]. Fifth, the signal-to- noise ratio is reduced by a factor of m for an m-spot image.

By combining two data collection strategies and two data processing strategies, we have at least four different routes to obtain time-resolved difference Fourier coefficients for each time point.

3. Results and discussions

3.1. *One-spot data set*

A one-spot image Laue data set was collected at 25 spindle angles separated by 4°. At each angle, diffraction patterns corresponding to the ground state and excited state (2 to 12 ms after laser off) were collected on separate image plates with 10 to 16 10 ms exposures for each, for a total exposure of 100 to 160 ms. One PYP crystal of size 50 × 50 × 450 μm was used for the entire data set. Spot streakiness (3 : 1 to 7 : 1 ratio of $a:b$) and numerous spatial overlaps were observed, but the analytical profile (Ren & Moffat, 1995*a*) fitted the diffraction spots successfully. The patterns were integrated to 1.6 Å resolution. Lorentz-factor and polarization corrections were applied and an isotropic scale factor and a temperature factor for each image were derived and applied. Wavelength normalization used the Chebyshev polynomial approach (Smith Temple, 1989; Ren & Moffat, 1995*a*). Table 1 is a summary of the single reflections. Energy-overlapped reflections were then deconvoluted (Ren & Moffat, 1995*b*) and yielded 3025 and 3065 unique reflections from the deconvolution for the ground state and excited state, respectively. Single reflections and deconvoluted multiples were then merged and compared with the PYP reference monochromatic data set (Table 2). The higher R factors between the Laue data set from the excited state and the monochromatic data set indicate a true signal arising from structural changes, rather than poorer data quality. Table 3 illustrates the completeness of these two subsets and the dependence of the R factors on resolution. The R factors at higher resolution are almost identical for the dark and excited states, which suggests the signal is being masked by noise at a resolution greater than 1.8 Å. Fig. 2 displays the $F_{\text{excited}} - F_{\text{ground}}$ Fourier map calculated from this one-spot image data set at 1.9 Å resolution. The native phase set (Borgstahl *et al.*, 1995) was used in the Fourier synthesis, but chromophore atoms (Baca, Borgstahl, Boissinot, Burke, Williams, Slater & Getzoff, 1994) and protein and solvent atoms in its vicinity were omitted in

Table 1. *Summary of integration and merging of Laue data sets (single reflections only)*

$$R \text{ factor} = \sum_{\mathbf{H}} \sum_{i=1}^{n_{\mathbf{H}}} (w_{\mathbf{H}i}|F_{\mathbf{H}i} - F_{\mathbf{H}}|) \Big/ \sum_{\mathbf{H}} \sum_{i=1}^{n_{\mathbf{H}}} (w_{\mathbf{H}i}F_{\mathbf{H}i}),$$

$$F_{\mathbf{H}} = \sum_{i=1}^{n_{\mathbf{H}}} (w_{\mathbf{H}i}F_{\mathbf{H}i}) \Big/ \sum_{i=1}^{n_{\mathbf{H}}} w_{\mathbf{H}i},$$

where $w_{\mathbf{H}i} = 1$ for unweighted R factors and $w_{\mathbf{H}i} = 1/\sigma^2(F_{\mathbf{H}i})$ for weighted R factors.

	One-spot		Two-spot	
	Ground	Excited	Ground	Excited
Number of images	25	24	23	23
Total observations	58791	52286	44542	41917
Unique reflections	9655	9435	6678	6706
Average redundancy	6.1	5.5	6.7	6.3
Integration resolution (Å)	1.6		1.9	
Wavelength range (Å)	2.0–0.7		2.0–0.7	
Merging R factor on F, unweighted (%)	7.4	7.9	7.1	7.5
Merging R factor on F, weighted (%)	4.9	5.2	4.7	4.9

Table 2. *Comparison of Laue data set (singles and multiples) with ground state monochromatic data set*

R factors are between the Laue data sets and the monochromatic ground state data set. See Table 1 for definition of R factors. The linear correlation coefficient is given by

$$\sum_{\mathbf{H}} ({}^{\text{Laue}}F_{\mathbf{H}} - {}^{\text{Laue}}F)({}^{\text{mono}}F_{\mathbf{H}} - {}^{\text{mono}}F) \Big/ \left\{ \left[\sum_{\mathbf{H}} ({}^{\text{Laue}}F_{\mathbf{H}} - {}^{\text{Laue}}F)^2 \right]^{1/2} \times \left[\sum_{\mathbf{H}} ({}^{\text{mono}}F_{\mathbf{H}} - {}^{\text{mono}}F)^2 \right]^{1/2} \right\}$$

where ${}^{\text{Laue}}F$ and ${}^{\text{mono}}F$ are means of ${}^{\text{Laue}}F_{\mathbf{H}}$'s and ${}^{\text{mono}}F_{\mathbf{H}}$'s for all **H**'s, respectively.

	One-spot		Two-spot	
	Ground	Excited	Ground	Excited
Common reflections	8950	8694	6702	6645
Resolution range (Å)	∞–1.6		∞–1.9	
Unweighted R factor on F (%)	7.1	7.9	7.9	9.7
Weighted R factor on F (%)	2.8	3.2	4.0	5.6
Linear correlation coefficient	0.9635	0.9535	0.9497	0.9260

the phase calculation. The largest features in the difference map are clustered at the chromophore site, as is chemically plausible, which suggests that these features are real.

3.2. *Two-spot data set*

A two-spot image data set was collected at the same two time points (ground state and excited state, 2 to 12 ms after laser off) but on the same detector frame with a small displacement between the images of 1.5 mm. Other conditions were identical to those used during collection of the one-spot image data set discussed above, except that the two-spot data set was collected at 23 spindle angles (23 images). One crystal of size 50 × 50 × 300 μm was used. The two-spot data set was integrated to 1.9 Å resolution, compared with 1.6 Å for the one-spot data set. This crystal appears to diffract more weakly, and the two-spot images have twofold higher noise.

On visually comparing these two Laue patterns on the same image plate, intensity reversals of adjacent spots are visible (Fig. 1*c*), which suggests a protein structural change. In order to extract this structural information, these Laue diffraction images must be accurately integrated. However, intensity changes due to a change in the underlying continuous molecular transform are often masked by time-dependent crystal mosaicity and mosaicity anisotropy. The left column of Fig. 3 is a portion of an experimental PYP two-spot image, in which the indices of the reflections are marked and the letters G and E denote the ground and excited states, respectively. The reflections from the ground state are less elongated, while the excited-state reflections are almost vertically elongated; that is, the spot profiles of the ground and excited states are quite different (Fig. 3). More seriously, one spot from the excited state may overlap with an adjacent spot from the ground state. By application of the profile-fitting technique described by Ren & Moffat (1995*a*) and in this paper, difficult situations like Fig. 3 can be solved accurately. The right column of the Fig. 3 shows the assembled, fitted profiles for the experimental image in the left column. That is, an experimental two-spot diffraction image is represented here by an analytical function of two groups of parameters that describe the intensity scales and the shapes of the spots. This profile-fitting technique removes random noise, deconvolutes spatial overlaps, integrates diffraction intensities and extracts crystal mosaicity information. The first three functions have been discussed by Ren & Moffat (1995*a*,*b*) and incorporated into the Laue data processing software *LaueView*, but the last function remains to be incorporated.

As described by Ren & Moffat (1995*a*) and above, each parameter in group 2 is a two-dimensional function of position in detector space, which can be represented by a surface. For one-spot images, the ground- and excited-state data can be treated as separate data sets in the integration process. For multiple-spot images, there is a more serious spatial overlap problem. The two-dimensional functions of shape-related parameters are allowed to differ for each Laue exposure on one frame. However, all functions are restrained to be smooth by the requirement that the standard profiles of adjacent detector bins for one exposure can differ only slightly. Fig. 4 shows examples of group 2 parameter surfaces for a two-

Table 3. *Completeness of the one-spot image data set (singles and multiples) and comparison with the monochromatic data set*

R factors are between the Laue data sets and the monochromatic ground state data set. See Table 1 for definition of *R* factors

	Ground state			Excited state		
	Completeness (%)			Completeness (%)		
Highest resolution (Å)	By shell	By sphere	*R* factor (shell, %)	By shell	By sphere	*R* factor (shell, %)
3.20	94.77	94.77	4.2	95.40	95.40	5.0
2.54	97.25	96.01	5.0	97.54	96.47	6.4
2.22	96.36	96.12	5.6	96.00	96.31	6.7
2.02	93.97	95.59	6.5	93.25	95.55	7.5
1.87	86.95	93.86	7.9	84.69	93.38	8.9
1.76	70.96	90.06	10.6	67.58	89.10	10.6
1.67	50.97	84.44	11.7	47.49	83.12	11.6
1.60	32.79	78.01	11.5	30.04	76.51	11.5

spot image in both the ground and excited states. The *a* surfaces (Figs. 4*a* and *b*) show that the length of streaky spots in the excited state is significantly longer than that of those in the ground state. The *b* surfaces (Figs. 4*c* and *d*) show less change in the width of spots. The value of ε, the nonradial correction angle (Ren & Moffat, 1995*a*), differs markedly (Figs. 4*e* and *f*) between the ground and excited states. These changes in the group 2 shape-related parameters apparently reflect time-dependent changes in the mosaicity and mosaicity anisotropy of the crystals. However, it is not yet clear whether the mosaicity changes arise solely from thermal artifacts induced by the laser illumination, or from time-dependent crystal lattice disorder induced by the protein structural change, or from both. Our analytical profile approach provides a useful tool to tackle the interesting problem of time-dependent crystal mosaicity. Finally, standard profiles of various spot shapes will have different integrals I_0 (Ren & Moffat, 1995*a*), as shown in Figs 4(*g*) and (*h*). This emphasizes that the diffraction intensity is related both to the parameter p_0 in group 1 and to the integral I_0 of the standard profile (Ren & Moffat, 1995*a*).

After integration, wavelength normalization and other correction factors were applied to the integrated intensities. Table 1 summarizes the results for the single reflections. Energy-overlap deconvolution (Ren & Moffat, 1995*b*) was again successfully applied and retrieved 592 and 570 unique reflections for the ground and excited states, respectively. Far fewer multiples are

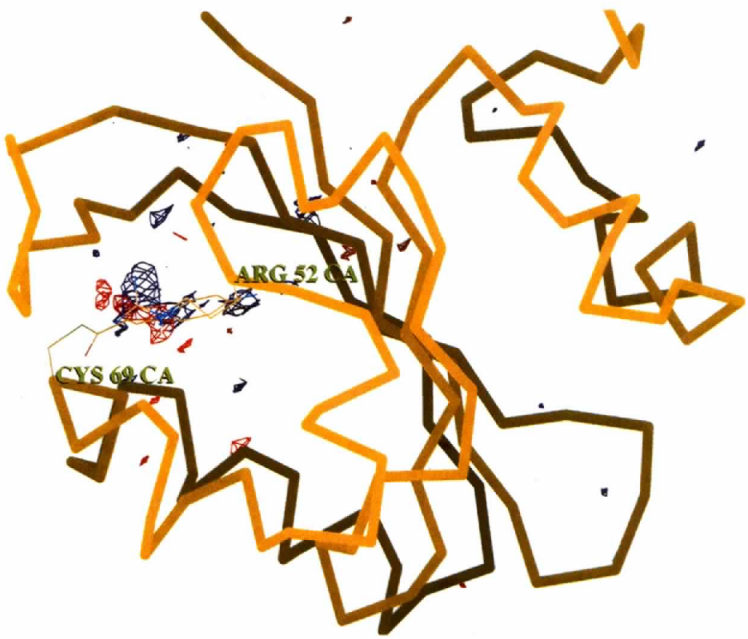

Fig. 2. The $F_{\text{excited}} - F_{\text{ground}}$ difference Fourier map of PYP at 1.9 Å resolution calculated from the one-spot image data set superimposed on the C_α-link trace of PYP in thick yellow. The difference coefficients are processed *via* the wavelength-normalization and harmonic-deconvolution route. The native phase set (Borgstahl *et al.*, 1995) is used in the Fourier summation but the chromophore and its vicinity are omitted in the phase calculation. The difference Fourier map is contoured at 3.5σ in red and -3.5σ in blue, where σ is the standard deviation of the entire map. The thin yellow lines show the structures of the side chains of the residues Arg52 and Cys69 as well as the covalent linked chromophore. The color levels indicate the depth of the objects. Ligher yellow colors indicate positions above the plane of the paper and darker green ones indicate positions below the plane of the paper (produced using *Xfit*/*XtalView*; McRee, 1992).

retrieved in the two-spot data set because the diffraction limit is much lower than in the one-spot data set. Tables 2 and 4 compare the monochromatic PYP data set and the merged Laue data sets. The completeness by resolution shell is listed in Table 4.

3.3. *Comparison*

As discussed earlier, by combining two data-collection routes, one- and two-spot images, and two data-processing routes, wavelength normalization and relative change, we obtain four different routes to difference Fourier coefficients. Table 5 compares the results from the four different routes. Different crystals naturally give diffraction images of different quality, and this is characteristic of realistic time-resolved experiments, where a single crystal is not sufficient to give the entire set of four-dimensional diffraction data. In order to accurately designate a spot in a Laue image as single or multiple (Cruickshank, Helliwell & Moffat, 1987), the true diffraction limit of the crystal must be identified (Ren & Moffat, 1995*a*), and Laue spots must be integrated to that resolution or slightly higher. Otherwise, the multiplicities of Laue spots will be assigned incorrectly. However, only those reflections common to all time points are useful for comparison. Therefore, the overall completeness of a time-resolved data set is limited by the poorest subset among those corresponding to each time point and by overlap between the subsets. We selected 2.1 Å as the resolution cutoff after several experimental trials because it seems to be the limit of useful signals in the two-spot image set. However, the one-spot image set contains signal up to 1.9 Å resolution. It is not surprising that the wavelength-normalization route applied to the one-spot data set retrieves 6.5% more unique reflections than the same route applied to the two-spot set, even at the same resolution of 2.1 Å. Unfortunately, the relative-change route applied to the one-spot data set is the least complete of the four strategies (Table 5); a Laue data set of higher resolution is more severely affected by the energy-overlap problem. It has been shown that the percentage of energy-overlapping reflections over all observed reflections is a constant that is independent of the diffraction limit of the crystal (Cruickshank *et al.*, 1987). Higher-resolution Laue data sets contain more energy overlaps and overlapping reflections are found at higher resolution too. Therefore, higher-resolution Laue data sets will have larger holes at low resolution. If energy overlaps cannot be deconvoluted accurately, reflections are inevitably going to be lost. Therefore, the wavelength-normalization route is a better choice, especially for data sets that extend to higher resolution.

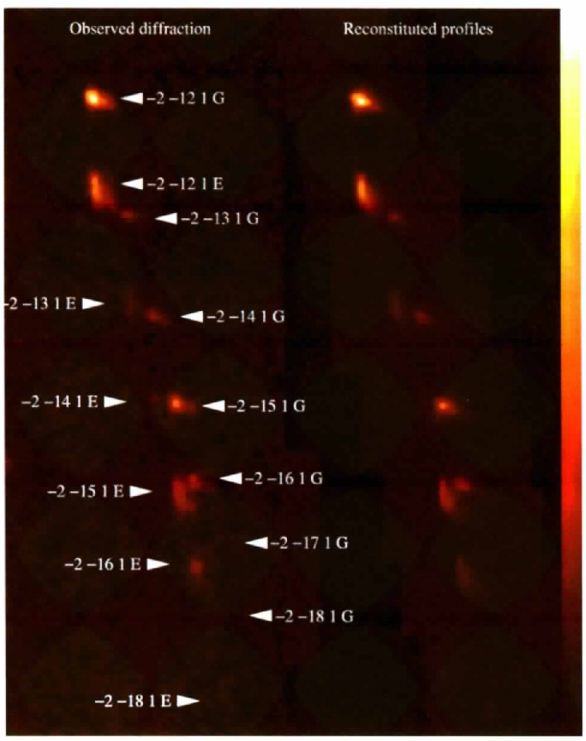

Fig. 3. Comparison of the real two-spot Laue image and the fitted profiles. The left column is a portion of a real PYP two-spot image with the indices and states marked. The letters *G* and *E* stand for the ground and excited states, respectively. The right column is the corresponding portion assembled from many individual profiles, each of which is a least- squares-fitted analytical profile. The profile shapes of the different states are allowed to be completely different, while those of the same state are only allowed to vary slowly across the image. Possible spatial overlaps are resolved by simultaneous fitting of several same or different profiles. Extremely weak reflections are also integrated by fitting the profiles to get the intensities that they deserve, but they do not contribute to the determination of the profiles.

Fig. 5 shows the $2F_o - F_c$ maps of the PYP chromophore site, where F_o is the structure-factor amplitude reduced from the ground-state Laue data sets and F_c is the structure-factor amplitude calculated from the refined model determined by monochromatic X-ray diffraction to 1.4 Å resolution (Borgstahl *et al.*, 1995). Figs. 5(*a*) and (*b*) are derived from the one-spot image set at 1.9 Å resolution and the two- spot image set at 2.1 Å resolution, respectively. The excellent match of this model, which was not refined against the Laue data sets, to the electron density calculated from the Laue data clearly demonstrates the Laue data quality.

Fig. 6 shows the $F_{\text{excited}} - F_{\text{ground}}$ maps for the six situations listed in Table 5. Again, a phase set was calculated from the same reference model (Borgstahl *et al.*, 1995) with the chromophore (Baca *et al.*, 1994) and its vicinity omitted, and the phases are not refined against any Laue data sets. These difference maps are contoured at $\pm 3\sigma$ levels, where σ is the localized standard deviation of the difference Fourier summation in an area distant from the chromophore site, in which only noise

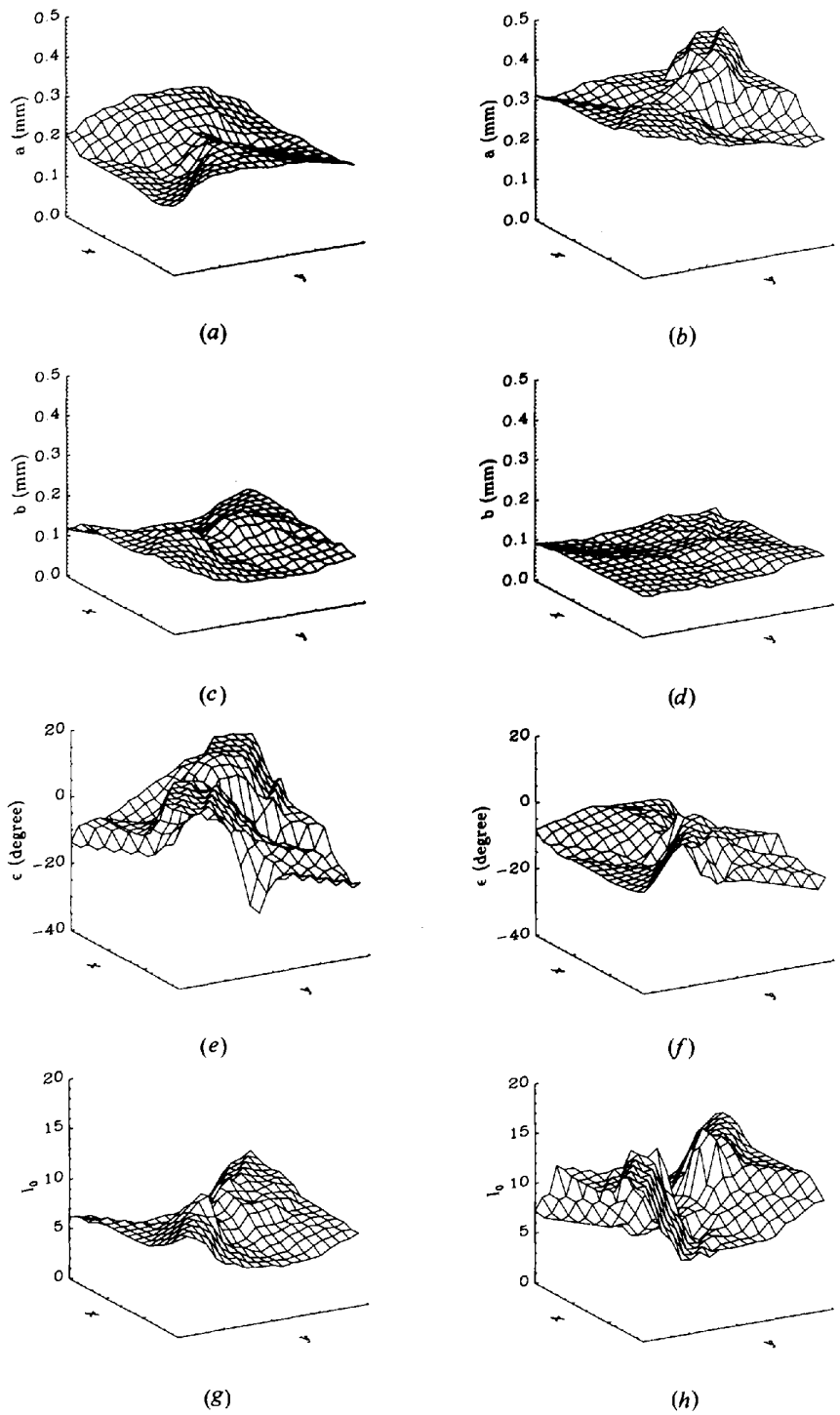

Fig. 4. Parameter surfaces of a PYP two-spot image. x and y are the coordinates of the detector bins. a and b are the half-long-axis and half-short-axis of the analytical profiles, respectively. ε is the nonradial streakiness correction angle. I_0 is the profile integral [see Ren & Moffat (1995*a*) for details]. (*a*) a surface of ground state; (*b*) a surface of excited state; (*c*) b surface of ground state; (*d*) b surface of excited state; (*e*) ε surface of ground state; (*f*) ε surface of excited state; (*g*) I_0 surface of ground state; (*h*) I_0 surface of excited state.

Table 4. *Completeness of the two-spot image data set (singles and multiples) and comparison with the monochromatic data set*

R factors are between the Laue data sets and the monochromatic ground state data set. See Table 1 for definition of *R* factors.

	Ground state			Excited state		
	Completeness (%)		*R* factor (shell, %)	Completeness (%)		*R* factor (shell, %)
Highest resolution (Å)	By shell	By sphere		By shell	By sphere	
3.80	93.48	93.48	5.6	93.13	93.13	6.6
3.12	95.99	94.72	4.4	96.44	94.77	6.3
2.63	93.22	94.22	6.2	93.22	94.25	8.4
2.39	93.38	93.51	8.0	91.73	93.62	9.8
2.22	90.19	92.84	10.1	90.39	92.97	12.0
2.09	84.27	91.42	11.9	83.28	91.36	13.3
1.99	74.45	89.00	13.8	75.15	89.05	15.3
1.90	57.48	85.03	15.2	56.83	85.00	16.9

Table 5. *Comparison of difference Fourier coefficient sets*

'Unique reflections' gives the numbers of difference Fourier coefficients $F_{excited} - F_{ground}$. For example, the first column statistics are based on the common reflections derived from the first two columns of Table 1 to the value of d_{min}* used. Unweighted *R* factors are between the Laue data sets of the ground and excited states. See Table 1 for definition of *R* factors.

	Wavelength-normalization route			Relative-change route		
	One-spot		Two-spot	One-spot		Two-spot
d_{min}* (integrated, Å)	1.6	1.6	1.9	1.6	1.6	1.9
d_{min}* (used, Å)	1.9	2.1	2.1	1.9	2.1	2.1
Unique reflections	7049	5382	4952	4489	3842	4027
Completeness (%)	85.6	87.7	81.2	54.6	63.1	66.2
R factor (%)	5.2	4.8	4.8	4.0	3.9	3.8
Figure	6(*a*)	6(*b*)	6(*c*)	6(*d*)	6(*e*)	6(*f*)

* Highest resolution

Table 6. *Comparison of time-resolved Laue data collection and processing routes*

	Advantages	Disadvantages
One-spot	Lowest noise, therefore highest resolution Minimum spatial overlaps	Most image files, therefore higher total readout noise Longer elapsed time for data collection Different time points collected far apart in real time, therefore prone to drift in source, optics *etc.*
Two-spot	Different time points collected close together on same frame, therefore less sensitive to drift Internal control on every observation Fewer image files Shorter elapsed time to collect	Greater background noise, therefore lower resolution Greater spatial overlaps
m-spot	Even fewer image files	Even greater background noise and spatial overlaps
Wavelength normalization	Energy-overlap deconvolution possible, therefore gives highest completeness, especially at low resolution	More complicated
Relative change	Less prone to drift	Cannot perform energy-overlap deconvolution, therefore poorer completeness Needs reference set, therefore longer total exposure time

supposedly exists. Basically, all the difference maps show the same features. The aromatic ring of the 4-hydroxycinnamyl chromophore (Baca *et al.*, 1994) leaves the blue density in the ground state and goes into the red density of '*S*' shape in its excited state. The side chain of Arg52 also leaves it ground state position. The details of the structural refinement, conformational changes and kinetics studies will be reported elsewhere (Ng, Borgstahl, Ren, Genick, Burke, Pradervand, Schildkamp, McRee, Getzoff & Moffat, 1996). The quality of these difference maps in real space agrees with our earlier analysis of the difference coefficients in reciprocal space. Higher-resolution data sets are less suitable for the percentage change route for difference Fourier coefficients. Figs. 6(*d*) and (*e*) for such situations are not as good as the others.

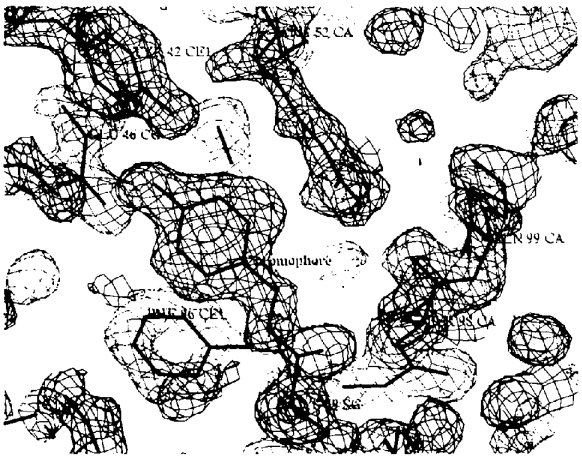

(*a*)

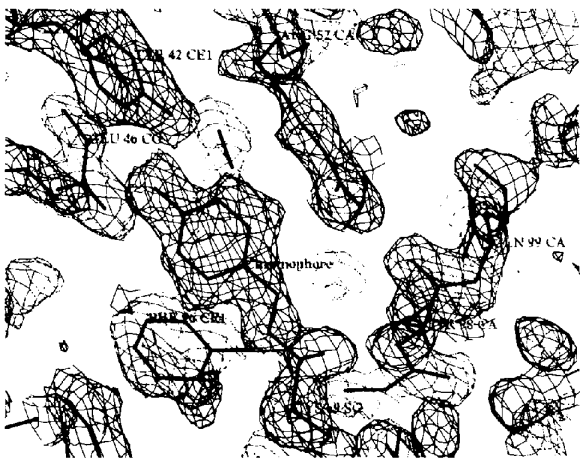

(*b*)

Fig. 5. The $2F_o - F_c$ Fourier maps of the PYP chromophore site superimposed on the native structure (Borgstahl *et al.*, 1995). F_o is the observed structure-factor amplitude reduced from the ground state Laue data set. F_c is the structure-factor amplitude calculated from the PYP native structure (Borgstahl *et al.*, 1995). The native phase set (Borgstahl *et al.*, 1995) is used in the Fourier summation but the chromophore and its vicinity are omitted in the phase calculation. The maps are contoured at 1σ, where σ is the standard deviation of the map. The extra contour at the site of Cys69 SG is at 7σ. The gray levels indicate the depth of the objects. Lighter grays indicate features located above the plane of the paper and darker ones those below. (*a*) one-spot image data set at 1.9 Å resolution; (*b*) two-spot image data set at 2.1 Å resolution (produced using *Xfit/XtalView*; McRee, 1992).

4. Concluding remarks

We have demonstrated that a new technique of profile fitting, using an analytical formula proposed by Ren & Moffat (1995*a*) and in this paper, could accurately carry out the spot integration for various Laue diffraction patterns. Two major problems in the integration of Laue diffraction spots, namely spot streakiness and spatial overlap, can be solved simultaneously. Multiple-spot images obtained in time-resolved experiments are more vulnerable to those problems. The analytical profile fitting has been demonstrated to be very suitable for such difficult spot deconvolution. This profile-fitting technique can obviously be extended to handle any two-dimensional spot integration in macromolecular crystallography, such as large-angle oscillation images (Weisgerber & Helliwell, 1993), where spatial overlap between adjacent spots could be severe or spot shapes could be far from standard.

We have compared the data quality of various data-collection and processing routes for time-resolved crystallographic studies. As long as wavelength normalization (Ren & Moffat, 1995*a*) and harmonic deconvolution (Ren & Moffat, 1995*b*) are used, one- and two-spot image data-collection strategies do not differ greatly from one another (Table 5). Two-spot images are more straightforward for direct inspection of diffraction intensity changes (Fig. 1) and may be acquired more quickly since the detector does not need to be interchanged and/or read out. Also, they yield fewer images to be read out. However, if changing the detector frame does not conflict with the timing of the two exposures, one-spot images would be expected to give better results since they have less noise owing to lower background and less complexity. One-spot image data sets also require minimum exposure time that will reduce radiation damage to the minimum, and they can be processed more conveniently owing to fewer spatial overlaps. The percentage-change strategy can only be applied to single nonenergy-overlapping reflections, which will sacrifice data completeness, and is particularly inappropriate for higher-resolution data sets. Table 6 summarizes the advantages and disadvantages of these routes.

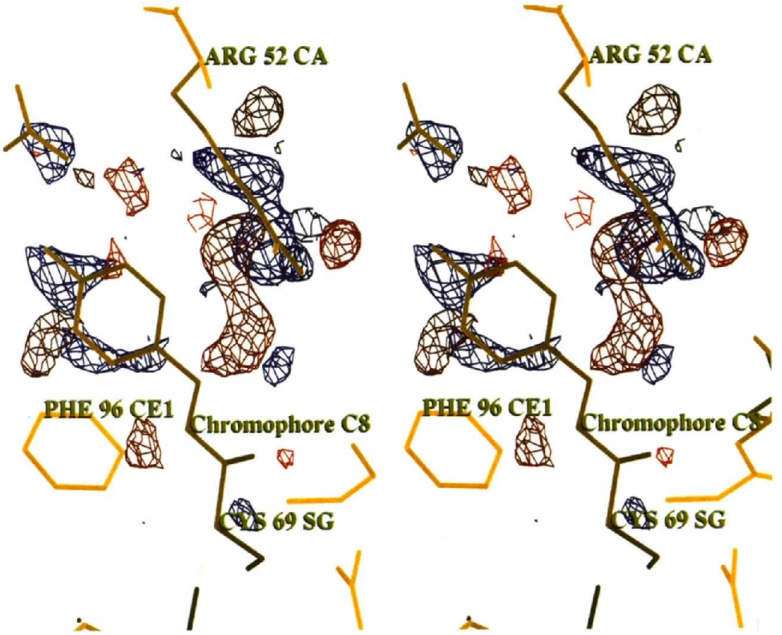

(*a*)

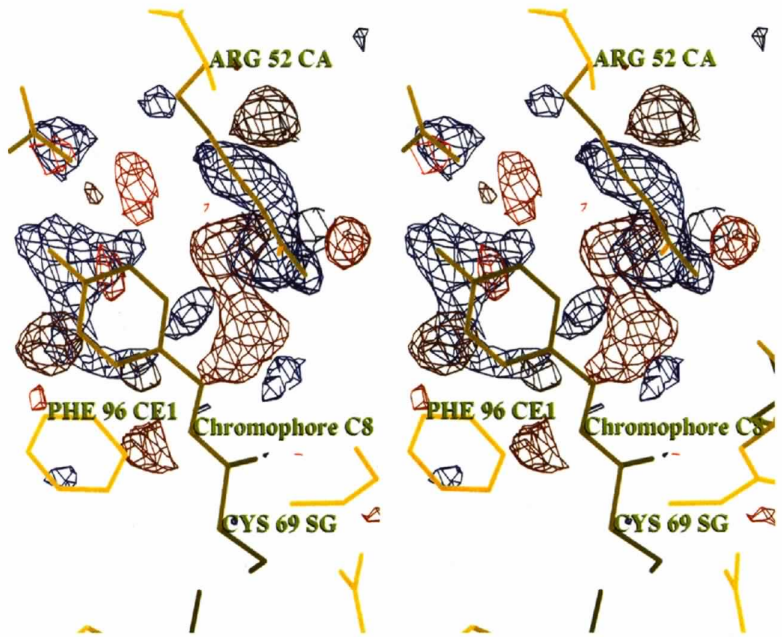

(*b*)

Fig. 6. The stereoview of $F_{excited} - F_{ground}$ difference Fourier maps of PYP superimposed on the native structure (Borgstahl *et al.*, 1995) in yellow. $F_{excited}$ and F_{ground} are reduced from the Laue data sets indicated in Table 5 for (*a*) to (*f*). The native phase set (Borgstahl *et al.*, 1995) is used in the Fourier summation but the chromophore and its vicinity are omitted in the phase calculation. The maps are contoured at 3σ in red and -3σ in blue, where σ is the localized standard deviation of each map in an area distant from the chromophore site, in which only noise supposedly exists (produced using *Xfit/XtalView*; McRee, 1992).

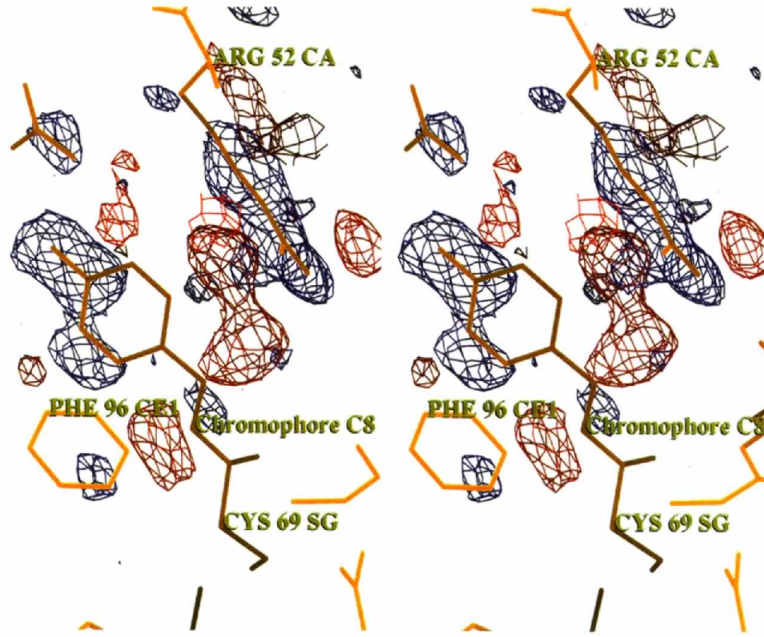
ARG 52 CA
PHE 96 CE1
Chromophore C8
CYS 69 SG
ARG 52 CA
PHE 96 CE1
Chromophore C8
CYS 69 SG

(*c*)

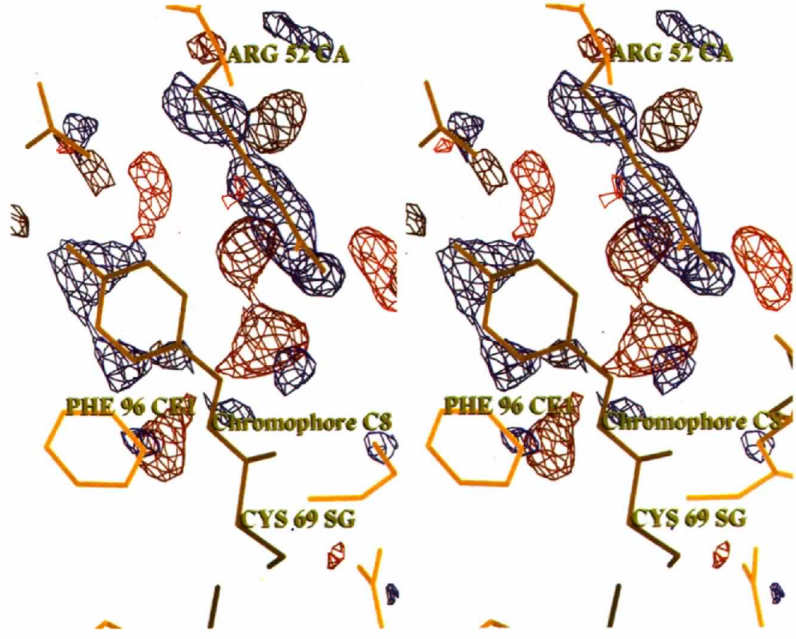
ARG 52 CA
PHE 96 CE1
Chromophore C8
CYS 69 SG
ARG 52 CA
PHE 96 CE1
Chromophore C8
CYS 69 SG

(*d*)

Fig. 6. (*cont.*)

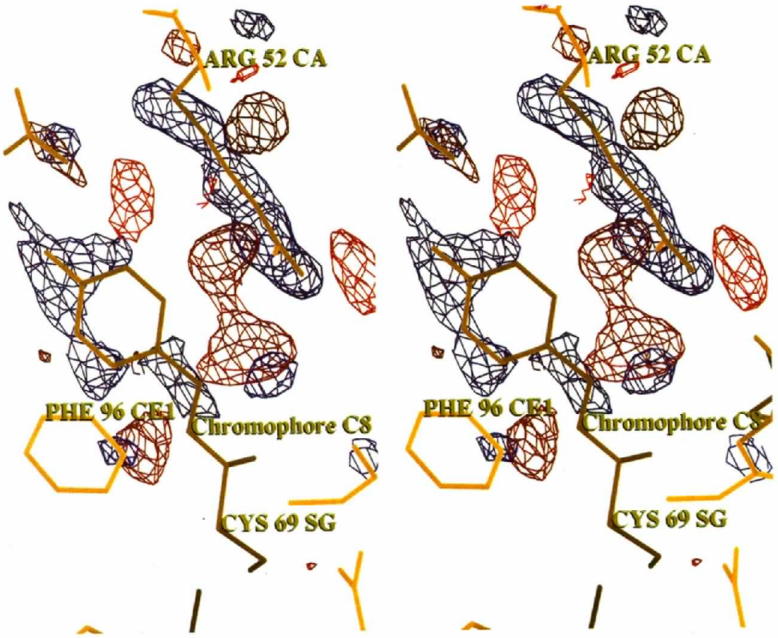
ARG 52 CA
PHE 96 CE1
Chromophore C8
CYS 69 SG
ARG 52 CA
PHE 96 CE1
Chromophore C8
CYS 69 SG

(*e*)

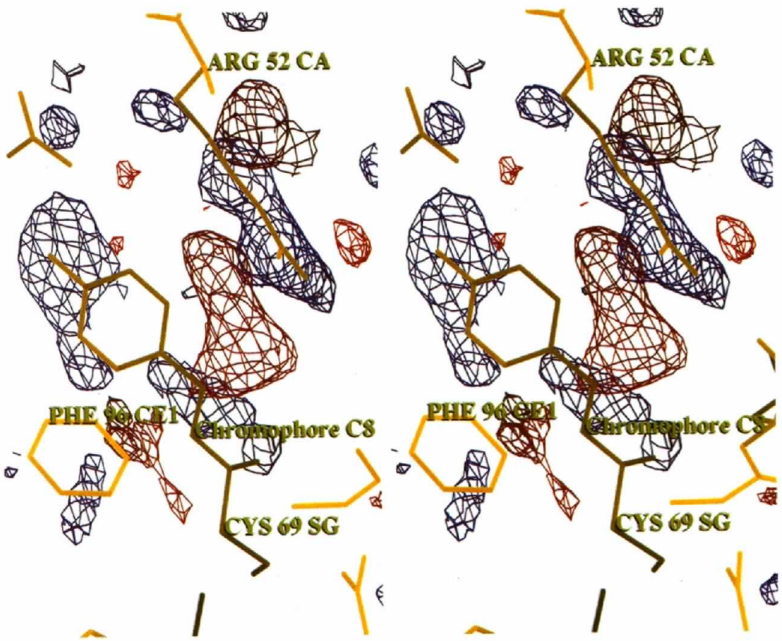
ARG 52 CA
PHE 96 CE1
Chromophore C8
CYS 69 SG
ARG 52 CA
PHE 96 CE1
CYS 69 SG

(*f*)

Fig. 6. (*cont.*)

We thank Drs W. Schildkamp, M. Rivers, K. Jones, A. LeGrand, T.-Y. Teng, V. Srajer and Y. Chen, and C. Pradervand and G. Shea McCarthy for building and maintaining beamline X26C at the National Synchrotron Light Source. Without their excellent apparatus, including the systems of X-ray shuttering and timing, the Laue camera, laser and on-line microspectrophotometer, the data discussed in this paper could not have been collected. We also thank Dr D. E. McRee and U. Genick for participation in data collection and for valuable discussions. This work is supported by grants from NIH to KM (GM 36452 and RR 07707) and EDG (GM 37684).

References

Baca, M., Borgstahl, G. E. O., Boissinot, M., Burke, P. M., Williams, D. R., Slater, K. A. & Getzoff, E. D. (1994). *Biochemistry*, **33**, 14369–14377.

Bartunik, H. D., Bartunik, L. J. & Viehmann, H. (1992). *Philos. Trans. R. Soc. (London) Ser. A*, **340**, 209–220.

Bilderback, D. H., Moffat, K. & Szebenyi, D. (1984). *Nucl. Instrum. Methods*, **222**, 245–251.

Borgstahl, G. E. O., Williams, D. R. & Getzoff, E. D. (1995). *Biochemistry*, **34**, 6278–6287.

Chen, Y. (1994). PhD thesis. Cornell University, Ithaca, New York, USA.

Cruickshank, D. W. J., Helliwell, J. R. & Johnson, L. N. (1992). Editors. *Time-Resolved Macromolecular Crystallography*. The Royal Society, Oxford University Press.

Cruickshank, D. W. J., Helliwell, J. R. & Moffat, K. (1987). *Acta Cryst.* **A43**, 656–674.

Getzoff, E. D., Jones, K. W., McRee, D., Moffat, K., Ng, K., Rivers, M. L., Schildkamp, W., Singer, P. T., Spanne, P., Sweet, R. M., Teng, T.-Y. & Westbrook, E. M. (1993). *Nucl. Instrum. Methods Phys. Res.* **B79**, 249–255.

Hajdu, J. & Andersson, I. (1993). *Ann. Rev. Biophys. Biomol. Struct.* **22**, 467–498.

Hajdu, D., Machin, P. H., Campbell, J. W., Greenhough, T. J., Clifton, I. J., Zurek, S., Gover, S., Johnson, L. N. & Elder, M. (1987). *Nature (London)*, **329**, 178–181.

McRee, D. E. (1992). *J. Mol. Graphics*, **10**, 44–46.

McRee, D. E., Meyer, T. E., Cusanovich, M. A., Parge, H. E. & Getzoff, E. D. (1986). *J. Biol. Chem.* **261**, 13850–13851.

McRee, D. E., Tainer, J. A., Meyer, T. E., Van Beeumen, J., Cusanovich, M. A. & Getzoff, E. D. (1989). *Proc. Natl. Acad. Sci. USA*, **86**, 6533–6537.

Meyer, T. E. (1985). *Biochem. Biophys. Acta*, **806**, 175–183.

Moffat, K. & Helliwell, J. R. (1989). *Topics Curr. Chem.* **151**, 61–74.

Moffat, K. (1989) *Annu. Rev. Biophys. Chem.* **18**, 309–332.

Moffat, K., Bilderback, D., Schildkamp, W. & Volz, K. (1986). *Nucl. Instrum. Methods Phys. Res.* **A246**, 627–635.

Moffat, K., Chen, Y., Ng, K., McRee, D. & Getzoff, E. D. (1992). *Philos. Trans. R. Soc. (London) Ser. A*, **340**, 175–190.

Ng, K., Getzoff, E. D. & Moffat, K. (1995). *Biochemistry*, **34**, 879–890.

Ng, K., Borgstahl, G. E. O., Ren, Z., Genick, U. K., Burke, P. M., Pradervand, C., Schildkamp, W., McRee, D. E., Gerzoff, E. D. & Moffat, K. (1996). In preparation.

Pai, E. F. (1992). *Curr. Opin. Struct. Biol.* **2**, 821–827.

Ren, Z. & Moffat, K. (1994). *J. Synchrotron Radiat.* **1**, 78–82.

Ren, Z. & Moffat, K. (1995*a*). *J. Appl. Cryst.* **28**, 461–481.

Ren, Z. & Moffat, K. (1995*b*). *J. Appl. Cryst.* **28**, 482–493.

Shrive, A. K. & Greenhough, T. J. (1994). *J. Appl. Cryst.* **27**, 532–542.

Smith Temple, B. R. (1989). PhD thesis. Cornell University, Ithaca, New York, USA.

Weisgerber, S. & Helliwell, J. R. (1993). *J. Chem. Soc. Faraday Trans.* **89**, 2667–2675.